Point-by-point reply from van Ramshorst et al. (2019) to: Review report: Wind speed measurements using distributed fiber optics: a wind tunnel study

Author of the paper: van Ramshorst et al.
Journal: Atmospheric Measurement Techniques
Manuscript DOI: 10.5194/amt-2019-63

General Comments

The study of van Ramshorst et al. investigated the actively heated fiber-optic (AHFO) technique and estimated its accuracy and precision under controlled airflow conditions by comparing to a three dimensional ultrasonic anemometer. A valuable error prediction equation for the wind speed measurements at different heating rates was developed, as the heating rate can be a limiting factor for long cables. This equation is also accounting for averaging over space or time which further increases precision. They conclude that AHFO measurements are reliable in outdoor deployments when correcting the measurements for directional sensitivity with a ultrasonic anemometer, choosing the right heating rate and spatial or temporal averaging. Distributed temperature sensing (DTS) measures temperatures along a fiber-optic cable spatially continuously and can be used in various fields. Especially for atmospheric research this technique offers new insight into the temperature field and thus was implemented in many studies. By using the AHFO technique, wind speed measurements can be added to the system. As the community using the DTS and AHFO technique is growing, the study of van Ramshorst et al. is important for users to be aware of the accuracy, precision and limitation of this technique. Hence, the paper is valuable for our community.
The author did do a good job on the first revision. The reviewed manuscript nicely rearranged the sections and made the manuscript more reader friendly. Also the additional turbulence statistics of the wind tunnel makes it a stronger manuscript. However, there are still some issues regarding precise description of the setup, definition of parameter, presentation of some graphs, and the error prediction function. Details are given below for each section. I recommend to accept the submitted manuscript after major revisions.

Thanks you for the positive feedback, we will give a point-by-point answers to your comments and questions below.

Terminology

- advective heat loss vs. convective heat loss: the correct terminology as is also used in the referenced literature of this manuscript is "convective".

We will change this accordingly.

Abstract & Section 1

- p.1, l.2-3: "...better characterization of fine-scale processes." - this is a very specific comment, but I think sonic anemometers can determine fine-scale processes better in time (20 Hz resolution vs. 1 Hz of DTS), while AHFO technique does have spatially continuously distributed measurements. Hence, AHFO can give inside into the wind field even a network of sonic anemometer might not be capable of on time scales > 1s. But I argue that a general statement like "better characterization" might not justify if not pointing out that the focus is on the spatial scale.

We agree that the benefits of the AHFO are mostly spatial, therefore we added the word spatial.

- p.1, l.4: "In this work, ..." this sentence is redundant

Agree, we removed the sentence

- p.1, l.6: "wind speed, angles of attack, and temperature differences" ! Oxford comma!

We changed this

- p.1, l.7: 1-s time scale

We changed this

- p.1, l.9: the correlation numbers can only be found in the abstract and conclusions, but not in the results section. Please refer to that correlation numbers in the result section, otherwise those high correlation numbers seem to come out of nowhere.

It is mentioned in the Accuracy and precision section on page 11, line 10 (old manuscript)

- p.1, l.11-12: "AHFO allows for characterization...complex terrain..." - AHFO can be deployed in any terrain, so I do not understand the focus on complex terrain. I would remove that sentence and only mention the last sentence which is way more important.

We removed the complex terrain part.

- p.2, l.3: "Goodberlet et al. (1989)" - aren't there also more recent paper commenting on that?

We added another more recent source

- p.2, l.16: 1-s and 0.3-m resolution

We changed this

- p.2, l.21-22: I do not understand the meaning of that sentence

We simplified the sentence

- p.2, l.25-27: the statements in those lines are very specific and belong into material and methods

We here describe the previous work of Sayde et al. and not our own set-up. Hence, we see this as an introduction part of our paper.

- p.2, l.29: magnitude of convective heat loss

We changed this

- p.2, l.31-25: This paragraph can be shortened: "The heat transfer model assumes a flow normal to the fiber. Hence, non-normal angles of attack need to be accounted for by using directional sensitivity equations. Following the recommendations of Sayde et al. (2015) we tested different directional sensitivity equations from hotwire anemometry in he controlled setting of our experiments" - or similar

We changed this sentence accordingly.

- p.3, l.7: remove "in complex terrain" - AHFO can be deployed in any terrain

We changed this

- p.3, l.13: "precision of future experiments" - precision of AHFO experiments

We changed this

Section 2.1 & 2.2

Both sections can be shortened by mentioning important literature and specifically focus on the parts which were changed in this manuscript to improve AHFO measurements. Section 2.2.1 has no new content and Figure 1 is from the paper of Sayde et al. (2015) altered in an incorrect way. The presented equations are also more or less a copy of Sayde et al. (2015). The most important changes are mentioned in Section 2.2.2, hence I would argue to remove Section 2.2.1 or only mention the most important points (like the energy balance) instead of the complete derivation of the equation determining the wind speed from AHFO measurements as already done by Sayde et al. (2015).

Section 2.2.1 contains indeed no new information and is a summary of the work of Sayde et al. (2015). We are already concise and we only introduce the parts we will change, as described in section 2.2.2. Accordingly, we think without this part the paper gets less readable. Also we changed advection to convection in figure 1.

I also have the following specific comments for those two sections:

- p.3, l.17-25: I think this paragraph is unnecessary for the manuscript focusing on AHFO. One sentence and pointing to the publication of Selker et al. 2006 is enough to explain the basic measurement principle of DTS. The last two sentences of the paragraph can be inserted somewhere else.

We agree and shorten this paragraph

- p.4, l.1: "heat the fiber" - heat the FO cable

We changed this

- p.4, l.2-3: "Also the creation of ..." - very confusing statement

We changed this

- p.4, l.6: "which van be" - which can be

We changed this

- p.4, l.10; p.5, l.5; p.5, l.13; p.5, l.14; ...: "advective" - "convective"

We changed this

Section 2.3

The whole section needs to be revised. Some information is unnecessary and could be addressed in one paragraph instead of mentioning it in different paragraphs. For example p.7, l.17-23 define the heating rates P_s creating ΔT for different wind speeds, however, the actually used ΔT are mentioned p.8 l.8 and the corresponding P_s p.9, l.1. Also the total number of experiments could be mentioned at the end after defining/mentioning all setups instead of consecutively summing up the experiment setups (p.8 l.2, l.6, l.8). Further, in this section FOs is used as a synonym for FO cable or FO cores, however, was not defined as such. The FO configuration as also introduced/proposed by Hausner et al. (2011) is introduced in p.8, l.10-11, then changed to a double-ended configuration (p.9, l.12), but actually a single-ended configuration (p.9, l.12) was used. This is more than confusing to the reader especially by mentioning it in different paragraphs. I would propose to mention the setup, only the actually chosen calibration method (as proposed by Hausner et al. (2011)), and step loss correction in one paragraph.

We revised the whole section and made it more concise according to your suggestions. We clarified if we mean the FO cable or FO core. We now only mention the single ended configuration.

I also have the following comments and questions:

- p.7, l.17-23: This paragraph should be revised. It is confusing to the reader. The main point should be the definition of the heating rate P_s fixing ΔT for different wind speeds. Accordingly, ΔT is representing P_s.

We changed this

- p.7, l.17: "The angle of the fiber..., wind speed, and heating rate were systematically changed" - This sentence is fine, however you start defining heating rate, then the angle of attack and then your wind speed settings... A reorganization makes it more reader friendly.

We changed this

- p.7, l.26-28: I am not sure if this sentence is important unless you add that those parts were excluded from analysis to avoid artifacts of the fiber touching the mounting material.

We think this should be part of the explanation of our set-up

- p.8, l.2: "The AHFO wind speed measurements can be calibrated..." – calibrated is not the correct use here, as DTS data itself is also calibrated. I suggest "adjusted" or "verified". Also removing that sentence would not affect the meaning of the paragraph.

We changed this

- p.8, l.10: The manufacturer of the FO cable is missing.

We added this

- Figure 3: The figure is not necessary for understanding the described method, Figure 2 is already showing the needed information. Either remove or put into Appendix.

We added this as an appendix

- p.9, l.1-6: this paragraph is describing the heating rate and how it can be estimated from the resistance of the FO cable. However, the heating rate is first mentioned p.7, l.22. I suggest to reorganize the section and to shorten this paragraph. The most important information is in the last sentence.

We changed this

- p.9, l.16. "splice loss": was a step loss correction performed?

Yes, according to Hausner et al. (2011).

Section 2.4 & Section 3.1

I do not completely agree with p.10, l.8-10. Sayde et al. (2015) never adjusted DTS measurements, they adjusted the sonic anemometer measurements and compared them to the AHFO measurements. Hence, the statement is not completely correct. However, I agree that the equation can be used to adjust for different attack angles and adjust/correct AHFO measurements if a sonic anemometer is near the AHFO setup. Figure 4 should be adjusted by showing violin plots or boxplots for each wind speed configuration. The shown dots cannot show the distribution of the DTS measurements in a clear way. Are real measurements of the sonics shown or the proposed fixed wind speeds?

We agree and rewrote the sentence about Sayde's correction method.

We changed figure 4 to boxplots. In our old plots the real measurements of the sonic was used, however in a boxplot this is not possible, and the proposed fixed wind speeds are used.

Section 3.2

The definition of σ_a and σ_p should be moved into material and methods. The result that σ_a and σ_p are dependent on wind speed and averaging over space and time and the corresponding discussion can remain in Section 3.2.

We added this to the method and a new short section.

On page 11 line 1-6 present details on the duplex FO configuration and that only the middle of the FO cable was used to estimate u_{DTS}, because otherwise the accuracy is decreased (Table C1). I think that this important piece of information, especially about the 90° attack angle, needs to be mentioned in Section 2.3. Further, shouldn't a step loss correction cover the effects of a splice?

We added this to the method. The reason we don't use part of the data is because of an asymmetrical splice loss. A step loss correction could correct also for the channel which looks wrong, however we do not want to introduce extra uncertainties.

I think Figure A1 and A2 are unnecessary as Figure 5 is giving the same information and derive the same conclusion. If the author decides to include those figures, they need to be adjusted in the same way as Figure 4.

We changed Figure A1 and A2 to boxplots.

Eq. 13 and 14 are presented in a confusing fashion by introducing dependencies which do not affect the definition of the introduced parameter. Eq. 13 and 14 define σ_a and σ_p, however, the definition itself is not reflecting any dependency on n_{space} nor n_{time}. This dependency is shown in Fig. 5 and Fig. 6 and should not be included in Eq. 13 and 14. The original equation from the first manuscript were better. Besides, the parameter u_j remains unclear to me as it also doesn't define σ_a and σ_p. Both are defined by u_{DTS} and u_{sonic}. I think u_j is introducing an unnecessary parameter. Further, Eq. 15 is introduced, which is changed to Eq. 16 without justification and both are different.

We agree and removed n_{space} and n_{time}. Also we changed the notation of Eq. 15 and Eq. 16. Furthermore, we changed uj to j, meaning a specific wind speed setting (1,3,5,7,9,11,13,15,16,17 m/s)

- p.12, l.12-14: those lines are redundant as they are already introduced on p.11, l.12-17

We agree and changed this

- p. 13, l.1-3: I do not see the justification of excluding the variation of sonic anemometer measurements by assuming it is small. If it was tested and did not change the results, I can see the justification of not considering that variation.

We show in appendix B (old manuscript) that there is low turbulence in the wind tunnel, therefore this term will be negligible, as our turbulence statistics are calculated with the sonic anemometer data.

Section 3.3 and Section 3.4

The title of Section 3.3 is not representing the content. The use of an intermediate constant is still not justified. The authors response to my comment did not include a justification nor the manuscript. The intermediate constant is defined as:

$$C_{int} = \overline{f(\bar{u}_j, n_{space}, n_{time}) * \frac{\Delta T}{T_{error}} * \sqrt{n_{time}}} \quad (1)$$

Hence, C_{int} (or $C_{DTS} = C_{int} * 10$) is the mean of the precision over a variation of setup:

$$C_{int} = \overline{\sigma_p * \frac{\Delta T}{T_{error}} * \sqrt{n_{time}}} \quad (2)$$

Those constants are then included in the estimation of σ_p again which is not justified. Besides, how was the factor T_{error} determined? Or is this number from literature? The revised manuscript is describing the derivation of the intermediate constant very quickly without further explanation. This should be presented in further detail. I still propose to derive the error prediction function in a more clear way. As shown in Fig. 6 for each ΔT the precision σ_p is following a $\frac{1}{\sqrt{n}}$-line. Hence, we assume the following dependency:

$$\sigma_p(n) = \frac{\alpha}{\sqrt{n}} \quad (3)$$

with α being a constant different for experiment set up. We found that α depends on ΔT and T_{error}:

$$\alpha = \left(\frac{\Delta T}{T_{error}}\right)^{-1} \quad (4)$$

with T_{error} = 0.25 K being the performance of the DTS dependent constant and ΔT being the measured temperature difference between the cables. Hence, α is representing the quality factor for the wind speed measurements. The lines derived from α could also be added in Fig. 6 or 7. When simplifying Eq. 20 of the submitted manuscript we can assume that ΔT is mainly depending on the following parameter:

$$\Delta T = \frac{AP_S}{Bu_n^m} \quad (5)$$

Combining my Eq. 4 and 5 and inserting that in Eq. 3, I derive the following error prediction equation:

$$\sigma_p(n, u_n, P_s) = \frac{BT_{error} u_n^m}{AP_s} \frac{1}{\sqrt{n}} \quad (6)$$

If I did not miss a point, no empirically derived intermediate constant has to be used for the error prediction equation.
I think the error prediction function could be tested with the existing data set by inserting P_s in the error prediction function and plotting that against the 'real' σ_p using Eq. 14 of the revised manuscript. This should show if C_{DTS} is needed or not.

We changed the title into Normalized precision independent of sampling settings, this represents the content of the section. T_{error} is determined from the machine specifications (page 14, line 8).

We understand your confusion, however we think our method is justified and the difference lies in Eq. 3 from you review. You state that σp is only dependent on the sampling n, however σp is also dependent on the wind speed (u). As can be seen in our eq. 14 (old manuscript). To confirm this with numbers we made some short calculations shown below, which shows that our CDTS factor makes the σp (for n_{time} = 30 sec) prediction more similar to the calculated observations from figure 6 (old manuscript). Therefore, we conclude that our method is correct and justified.

Table 1: Comparing van Ramshorst et al. and review report way of calculating σ_p, for comparison with Figure 6 (old manuscript); Values calculated for n_{time} = 30.

Angle	*ΔT*	*σ_p - van Ramshorst et al.; eq. 22*	*σ_p - Review report; eq. 6*
90°	6	0,0162	0,0032
45°	4	0,0190	0,0038
30°	2	0,0418	0,0084
15°	4	0,0345	0,0069

Section 3.5 & conclusions & Appendix

Section 3.5 is not introducing new content. It should be incorporated in the corresponding sections as a paragraph of discussion or incorporated into the conclusions if the statement is more an outreach than a finding.

Since section 3 is results and discussion we think it is appropriate to have a separate section which puts the results in perspective and gives a short outreach.

- p.17, l.19-20: how can turbulence be fully captured by the AHFO technique? Which turbulence scales are you talking about? How should the setup look like?

We clarified this, we meant larger scale turbulence depending on your spatial and temporal sampling resolution, but at least > 1s and > 0.3m.

- p.18, l.6-7: "Due to the way this design tool is constructed, it can be generalized for all kinds of fibers, DTS precisions, and user preferred spatial and temporal resolution." I do not agree with this statement, because the accuracy and precision of the DTS measurements change with the use of FO cable, DTS performance, and the used calibration method. Further, the turbulence of the wind tunnel setup does not represent outdoor turbulence as also stated in this manuscript. Another point is the response time of the FO cable. The thicker the cable, the longer it takes to reach the FO core and measure the temperature change. Also the measurement location of the wind speed is important, as the noise of measurement increases with distance from the measurement device, hence with the location along the FO cable. So how should C_{DTS} and the error prediction function be representative for outdoor deployments, different choice of FO cable, different setup of FO cable, or a different DTS machine? I think the statement is too strong and not justified.

We partly agree and downscaled our statement a bit. However, we also partly disagree and in our opinion the following things are included:

- *the thickness of the cable is in parameter A and B; eq. 22 (old manuscript)*
- *The DTS performance, calibration and cable length can be adjusted with T_{error}*

We agree that the turbulence is not included, although we should take into account that this is a first estimate, not a fully describing function of σ_p.

- p.18, l.11: "...applications in complex terrain, allowing for..." -...applications, for example allowing for... - AHFO can be deployed in any terrain.

We changed this

- Figure B2: turbulence intensity should be defined in the caption, as well as the location of the x-, y- and z-coordinate.

We clarified this in the appendix

Revisiting wind speed measurements using actively heated fiber optics: a wind tunnel study

Justus G.V. van Ramshorst[1,4], Miriam Coenders-Gerrits[1], Bart Schilperoort[1], Bas J.H. van de Wiel[2], Jonathan G. Izett[2], John S. Selker[3], Chad W. Higgins[3], Hubert H.G. Savenije[1], and Nick C. van de Giesen[1]

[1]Delft University of Technology, Water Resources Section, Stevinweg 1, 2628 CN Delft, The Netherlands
[2]Delft University of Technology, Geoscience and Remote Sensing, Stevinweg 1, 2628 CN Delft, The Netherlands
[3]Oregon State University, Biological and Ecological Engineering, 116 Gilmore Hall, Corvallis, Oregon 97331, USA
[4]University of Göttingen, Bioclimatology, Büsgenweg 2, 37077 Göttingen, Germany

Correspondence: Justus van Ramshorst (justus.vanramshorst@uni-goettingen.de)

Abstract. Near-surface wind speed is typically only measured by point observations. The Actively Heated Fiber-Optic (AHFO) technique, however, has the potential to provide high-resolution distributed observations of wind speeds, allowing for better spatial characterization of fine-scale processes. Before AHFO can be widely used, its performance needs to be tested in a range of settings. In this work, experimental results on this novel observational wind-probing technique are presented. We utilized a controlled wind-tunnel setup to assess both the accuracy and the precision of AHFO under a range of operational conditions (wind speed, angles of attack and temperature difference). The technique allows for wind speed characterization with a spatial resolution of 0.3~~m on a 1 s~~ -m on a 1-s time scale. The flow in the wind tunnel was varied in a controlled manner, such that the mean wind, ranged between 1 and 17 ms^{-1}. The AHFO measurements are compared to sonic anemometer measurements and show a high overall correlation (0.94-0.99). Both the precision and accuracy of the AHFO measurements were also greater than 95% for all conditions. We conclude that the AHFO has potential to measure wind speed and we present a method to help for choosing the heating settings of AHFO. AHFO allows for characterization of spatially varying fields of mean wind~~in complex terrain, such as in canopy flows or in sloping terrain~~. In the future, the technique could be combined with conventional Distributed Temperature Sensing (DTS) for turbulent heat flux estimation in micrometeorological/hydrological applications.

1 Introduction

This work presents the results of a wind tunnel study designed to test the novel Actively Heated Fiber-Optic (AHFO) (Sayde et al. (2015)) wind speed measurement technique in controlled airflow conditions. The primary aims of the experiment were to assess the directional sensitivity and signal-to-noise ratio of AHFO.

Wind speed is most commonly observed using in-situ point measurement techniques. As a result, the spatial distribution of field observations is limited. While it is possible to obtain distributed wind speed observations with remote sensing (e.g., Goodberlet et al. (1989); Bentamy et al. (2003)), the spatial resolution is too low for many micrometeorological applications.

Many field experiments assume Taylor's frozen flow hypothesis (Taylor (1938)) in order to estimate fluxes with similarity theory (e.g., Higgins et al. (2009); Kelly et al. (2009); Bou-Zeid et al. (2010); Patton et al. (2011)). However, similarity theory only holds for idealized homogeneous/stationary conditions, which are rarely met in practice, resulting in a model containing strong assumptions, which often leads to significant errors (Ha et al. (2007); Higgins et al. (2012); Thomas et al. (2012)). In real, non-idealized situations, even slight surface heterogeneities can lead to dramatic impacts on the spatial structure of the flow in the surface boundary layer. Further, even if perfect surface homogeneity was possible, other atmospheric (surface) conditions are often nonstationary as well (Holtslag et al. (2013)).

In the past decade, a new way to obtain spatial distributed measurements was introduced into environmental studies. High spatial resolution measurements could be used to check underlying assumptions and would reduce the need for such assumptions in real-world cases. Distributed Temperature Sensing (DTS) technology measures temperature at high temporal and spatial resolution over distances of up to several kilometers by using Fiber Optic (FO) cables as sensors (Selker et al. (2006a); Selker et al. (2006b); Tyler et al. (2009)). High-end DTS can measure the temperature at a ~~1 s~~ 1-s and 0.3~~m~~ -m resolution (Sayde et al. (2014)). The ability to report temperature at such high resolution has proven useful in many environmental studies (Selker et al. (2006a); Selker et al. (2006b); Tyler et al. (2008); Tyler et al. (2009); Steele-Dunne et al. (2010)), including atmospheric experiments (Keller et al. (2011); Petrides et al. (2011); Schilperoort et al. (2018); Higgins et al. (2018); Izett et al. (2019)). It has also been shown that it is possible to observe air temperature and thermal structure of near-surface turbulence with DTS (Thomas et al. (2012); Euser et al. (2014); Zeeman et al. (2015), Jong et al. (2015)).

Recently, Sayde et al. (2015) introduced the AHFO technique ~~as a means of performing independent explicit wind speedmeasurements using distributed temperature sensing (DTS) technology~~where they aimed to use DTS to measure wind speed. The underlying concept of the proposed method is similar to that of a hotwire anemometer; however, instead of single point measurements, AFHO enables distributed measurements to be made at high spatial resolution. Instead of only passively measuring the temperature in the fiber (as is done with DTS), one segment of the cable is actively heated. The heated segment is positioned parallel to the unheated reference segment, with a small separation, in our case 0.1 m. The temperature difference between the heated and reference segment is measured, i.e., the heated fiber and the air temperature. The temperature difference between the cables depends on the energy input as well as on the wind speed of the ambient air, which determines the magnitude of the lateral heat exchange, through convective heat loss. By setting up an energy balance for the heated cable, one can estimate the magnitude of this ~~advective~~ convective heat transport, which leads to an estimate of the wind speed.

Results from a field study by Sayde et al. (2015) demonstrated promising performance of the AHFO technique, but they recommended further tests on two aspects to be performed in controlled airflow conditions. First, the heat transfer model assumes ~~the flow is~~ a flow normal to the axis of the fiber. ~~Sayde et al. (2015) developed a first-order estimate of the influence of a~~ Hence, non-normal ~~angle of attack (the difference between the wind direction and the axis of the fiber), using a directional sensitivity equation~~ angles of attack need to be accounted for by using directional sensitivity equations. Following the recommendations

of Sayde et al. (2015) we tested different directional sensitivity equations from hotwire anemometry (Webster (1962); Hinze (1975); Perry (1982); Adrian et al. (1984)) ~~, but it needs to be tested in a controlled setting to determine its validity~~in the controlled setting of our experiment. Second, Sayde et al. (2015) highlight the importance of a sufficient signal-to-noise ratio when conducting measurements. They show that the temperature difference between the heated and reference segments gives a good estimate for this ratio. The influence of the directional sensitivity and the signal-to-noise ratio on the measurement accuracy and precision is investigated and the results are used to propose a method to estimate the precision for future experiments with AHFO, hence our work will improve the possibilities for successful application of AHFO in future field experiments.

Finally, in the future it will be interesting to perform outdoor tests with AHFO~~in complex terrain~~, for both micrometeorological and hydrological applications, as AHFO gives a lot of insights in spatial varying wind fields. AHFO can be especially interesting in non-homogenous field sites, like forests, which are already studied with other DTS applications (Schilperoort et al. (2018)). Moreover, the ability to measure spatial varying wind fields can be useful for estimating sensible heat fluxes in a variety of atmosphere-vegetation-soil continuums.

An overview of the experimental setup is presented in ~~section~~ Section 2, with the accuracy and precision of the AHFO experiments presented in ~~section~~ Section 3. In ~~section 4~~Section 3.4, a method for estimating the precision ~~for future~~ of AHFO experiments is introduced, followed by a short note on future studies.

2 Experimental Set-Up and Methods

2.1 DTS and Signal-to-Noise ratio analysis

Based on the backscattered signal of a laser pulse inside fiber optic cables, a Distributed Temperature Sensing (DTS) machine measures temperature along a complete fiber optic cable (Selker et al. (2006a); Selker et al. (2006b)). ~~These fiber optic cables can have lengths up to several kilometers with a spatial resolution down to 0.3 m, i.e., one DTS machine makes to thousands of near-simultaneous individual measurements. Laser pulses are sent with a fixed wavelength and most backscattered light keeps this wavelength, however some backscattered laser shifts to a shorter or longer wavelength, these frequency-shifted reflections are referred to as Raman-backscatter (Selker et al. (2006a)). By counting the backscattered photons with a longer (Stokes) and shorter (Anti-Stokes) frequency, a ratio between these two can be calculated. The strength of the Anti-Stokes signal depends on temperature, hence the ratio between the power of the Stokes and Anti-Stokes changes with temperature. This principle is used to measure the temperature along the cable. Consequently, a~~ A main source of noise in DTS data is white noise induced by the statistical variability in photon count from backscatter (optical shot noise). The white noise can be reduced by averaging over multiple measurements in either space or time, assuming the observed temperature is/stays (relatively) constant ~~van de Giesen et al. (2012)~~(van de Giesen et al. (2012)).

A sufficiently high signal-to-noise ratio is essential for measurement precision with DTS. In Sayde et al. (2015) it is shown that the signal-to-noise ratio can be described as: $(T_s - T_f)/T_{error}$, where T_s and T_f are the temperature (in K) of the heated cable segment and (unheated) reference segment (i.e., air temperature). Hence the signal-to-noise ratio is related to the ΔT (= $T_s - T_f$) and the measurement error of the DTS, T_{error} (in this study at a ~~1 s~~ 1-s sample resolution). A large ΔT is obviously

desirable, however, ΔT cannot be increased infinitely. The power controller can only deliver a limited amount of power to heat the ~~fiber~~FO cable, which is especially relevant for the heating of long lengths of FO cable (i.e. several hundreds of meters of FO cable). ~~Also the creation of~~ Additionally larger temperature differences ~~means the importance of~~ can cause that other ways of transferring energy ~~changes~~ (e.g., free convection, radiation and diffusion) can become more dominant/important. The effect of ΔT is investigated by using three temperature differences during the experiment. The effect of the signal-to-noise ratio is quantified, and an equation to estimate the precision is presented. The measurement precision is an indication of the variability of wind speed measurements (e.g., RMSD), as opposed to accuracy which describes a systematic measurement error for which ~~van~~ can be compensated (in our case expressed by the bias).

2.2 Determination of Wind Speed

2.2.1 Original determination of Wind Speed by Sayde et al. (2015)

An energy balance is used to quantify the heat dissipation from the heated section, and therefore estimate the wind speed with DTS. The ~~advective~~ convective cooling can be converted to wind speed, because it is a function of wind speed and the temperature difference between the heated and unheated segments. The full energy balance (in W) for a cable segment volume of length, B, is given by Sayde et al. (2015), and schematically shown in Figure 1:

$$c_s \rho_v V \frac{\mathrm{d}T_s}{\mathrm{d}t} = P_s B + (\bar{S}_b + \bar{S}_d + \alpha_s \bar{S}_t)(1-\alpha_f) 2r\pi B + (\bar{L}_\downarrow + \bar{L}_\uparrow)\epsilon 2r\pi B - \epsilon\sigma T_s^4 2r\pi B - h(T_s - T_f)2r\pi B \quad (1)$$

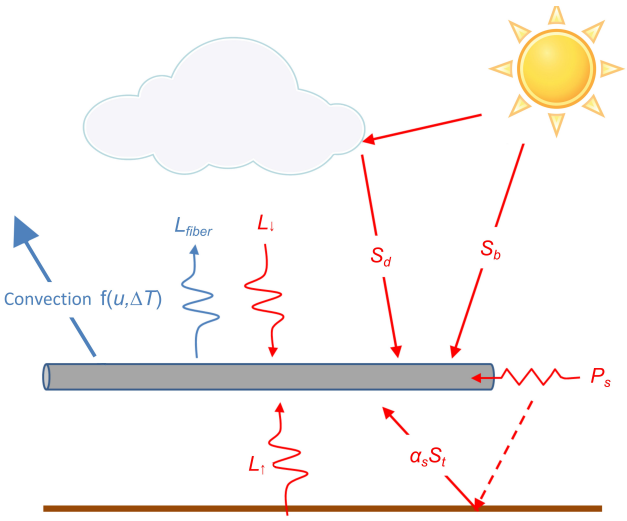

Figure 1. Schematization of the energy balance, based on Sayde et al. (2015)

Where, r is the radius of the cable ($6.7 \cdot 10^{-4}$ m in our setup); V is the volume of the cable segment ($\pi r^2 B$, in m^3), c_s is the specific heat capacity of the FO cable (502 $Jkg^{-1}K^{-1}$) and ρ_v is the FO cable density (800 kgm^{-3}). P_s is the heating rate per meter of cable (in Wm^{-1}); and B is the length of a cable segment (in m). $\bar{S}_b, \bar{S}_d$ and $\alpha_s \bar{S}_t$ (in Wm^{-2}) are the mean direct, diffuse and reflected short wave radiation fluxes, respectively, with α_s being the surface albedo of the ground; and α_f is the FO cable optic surface albedo. $\bar{L}_\downarrow + \bar{L}_\uparrow$ (in Wm^{-2}) are the average downward and upward longwave radiation fluxes, respectively; and ϵ is the FO cable surface emissivity. Based on the kind of stainless steel, emissivity values can range from 0.3 to 0.7 (Baldwin and Lovell-Smith (1992)); however, we assume a value of 0.5 (Madhusudana (2000)). σ is the Stefan-Boltzmann constant, $5.67 \cdot 10^{-8}$ (Wm^{-2} K^{-4}); and $\epsilon\sigma T_s^4$ is the outgoing longwave radiation of the fiber, i.e., L_{fiber}; h is the ~~advective~~ convective heat transfer coefficient ($Wm^{-2}K^{-1}$).

Simplification

The energy balance is simplified, by dividing Eq. 1 by $2r\pi B$, which is equal to the surface area of the FO cable. The energy balance now no longer depends on B, meaning the length of FO cable segment does not need to be defined. The proposed final energy balance by Sayde et al. (2015) is as follows and in Wm^{-2}:

$$\frac{c_s \rho r}{2} \frac{\mathrm{d}T_s}{\mathrm{d}t} = \frac{P_s}{2\pi r} + (\bar{S}_b + \bar{S}_d + \alpha_s \bar{S}_t)(1 - \alpha_f) + (\bar{L}_\downarrow + \bar{L}_\uparrow)\epsilon - \epsilon\sigma T_s^4 - h(T_s - T_f) \tag{2}$$

where, ρ is the FO cable density per meter of cable segment: 4.5 x 10^{-3} kgm^{-1}.

~~Advective~~ Convective heat transfer coefficient

The ~~advective~~ convective heat transfer coefficient h ($Wm^{-2}K^{-1}$) can by means of the dimensionless Nusselt (Nu), Prandtl (Pr), and Reynolds (Re) numbers be expressed as function of the wind speed, $h = f(u_n)$. The Nusselt number is the ratio between the advective and conductive heat transfer, where the Nusselt number can be written as follows (Žukauskas (1972)):

$$\mathrm{Nu} = \frac{h d_s}{K_a} = C \mathrm{Re}^m \mathrm{Pr}^n \left(\frac{\mathrm{Pr}}{\mathrm{Pr}_s}\right)^{\frac{1}{4}} \tag{3}$$

with,

$$\mathrm{Re} = \frac{u_n d_s}{\upsilon_a} \tag{4}$$

d_s is the fibers characteristic length ($2r$); K_a is the thermal conductivity of air and υ_a the kinematic viscosity of air, respectively 0.0255 $Wm^{-1}K^{-1}$ and 1.5 x 10^{-5} m^2s^{-1} (Tsilingiris (2008)). K_a and υ_a are assumed to be constant, due to the controlled conditions in the wind tunnel, but in field experiments this should be included as a variable, as K_a and υ_a are temperature and relative humidity depend (Tsilingiris (2008)). C, m and n are empirical constants related to forced advection of heat by air movement. In Sayde et al. (2015), C, m and n values of 0.51, 0.5 and 0.37 are set, based on (Žukauskas (1972)). Pr is the Prandtl number and can be seen as the ratio between kinematic viscosity and thermal diffusivity, which, we assume Pr to be

constant (0.72) for our range of temperatures (12-35 K), as in Tsilingiris (2008), with Pr_s (the Prandtl number for the heated fiber segment), assumed to be the same as Pr, due to the small temperature differences (max. 6 K). Lastly, Re is the Reynolds number which is used to determine the flow regime of the air along the fiber segments, i.e., Re expresses if the flow regime is laminar or turbulent. Combining Eq. 3-4 yields:

$$h = C d^{m-1} \mathrm{Pr}^n \left(\frac{\mathrm{Pr}}{\mathrm{Pr}_s}\right)^{\frac{1}{4}} K_a \upsilon_a^{-m} u_n^m \tag{5}$$

The determination of the Nusselt number (Eq. 3) is only valid in the following ranges of Re (40-1000) and Pr (0.7-500). Re can be a limitation for higher wind speeds, especially when the diameter of the fiber is large, in our case wind speeds higher than approximately 11 ms^{-1} would be out of range. In the derivation of the energy balance (1), there is assumed to be no free convection, induced by heating of the air close to the cable, and no conduction of heat in the axial direction of the FO cable. It is also assumed there is no radiative exchange between objects close and parallel to the heated fiber, i.e., dispersion of heat from the heated cable to the reference cable is assumed to be negligible. Furthermore, a flow directed normal to the axis of FO cable is assumed by the proposed energy balance, i.e., for flow directed in a different angle, compensation is necessary to accurately estimate the wind speed.

2.2.2 Revised simplified determination of Wind Speed

Due to the setup inside the wind tunnel, as opposed to outdoor conditions, some simplifications can be made. The short wave radiation can be neglected because it is an indoor experiment (no sunlight). Furthermore, we assume that there is a uniform temperature inside the wind tunnel, due to the enclosed conditions. This means the incoming radiation is dependent on the air temperature, T_f. Assuming incoming ($\bar{L}_\downarrow + \bar{L}_\uparrow$) to be black body radiation (i.e., $L_{in} = \sigma T_s^4$), the net longwave radiation loss for the fiber can be simplified accordingly by merging the incoming longwave and outgoing longwave radiation as:

$$(\bar{L}_\downarrow + \bar{L}_\uparrow)\epsilon - \epsilon\sigma T_s^4 \approx -\epsilon\sigma(T_s^4 - T_f^4) \tag{6}$$

One more additional change is made, based on our results obtained during testing of the performance of the AHFO technique. In processing of the obtained wind tunnel data it was found that by using the calculation of the Nusselt number from Žukauskas (1972), Eq. 3, a $\sim 20\%$ additional bias in calculating the wind speed was created. By using a more recent version for calculating the empirical Nusselt number (Cengel and Ghajar (2014)), the bias in our study is reduced to $\sim 5\%$ Therefore, Eq. 7 is proposed to calculate the Nusselt number, where the constants C, m and n are still used; however, with the values from Table 7-1 ($C = 0.683, m = 0.466$ and $n = 1/3$) in Cengel and Ghajar (2014), rather than those in Žukauskas (1972). Next to the improved fit, the range of Re over which the equation is valid is much wider (40-4000 compared with 40-1000), and therefore more applicable in future AHFO experiments.

$$\mathrm{Nu} = C\mathrm{Re}^m\mathrm{Pr}^n = 0.683\mathrm{Re}^{0.466}\mathrm{Pr}^{1/3} \tag{7}$$

Consequently, the expression of h changes as well.

$$h = Cd^{m-1}\mathrm{Pr}^{n}K_a\upsilon_a^{-m}u_n^{m} \tag{8}$$

With the long- and short-wave radiation simplifications, the energy balance becomes:

$$\frac{c_s\rho r}{2}\frac{\mathrm{d}T_s}{\mathrm{d}t} = \frac{P_s}{2\pi r} - \epsilon\sigma(T_s^4 - T_f^4) - h(T_s - T_f) \tag{9}$$

By substituting the expression for h (Eq. 8), we can rearrange Eq. 9 to obtain an expression for wind speed. Eq. 10 will be used to estimate the wind speed (u_N) in our wind tunnel study.

$$u_N = \left(\frac{0.5P_s\pi^{-1}r^{-1} - \epsilon\sigma(T_s^4 - T_f^4) - 0.5c_p\rho r\frac{\mathrm{d}T_s}{\mathrm{d}t}}{Cd^{m-1}\mathrm{Pr}^{n}K_a\upsilon_a^{-m}(T_s - T_f)}\right)^{1/m} \tag{10}$$

2.3 Wind tunnel experiments

We conducted a series of experiments under tightly controlled airflow conditions to improve the applicability of AHFO in experimental (field) research and to study the directional sensitivity and influence of the signal-to-noise ratio. The experiments presented were performed in a wind tunnel at Oregon State University. This wind tunnel has a closed circuit, which means the air inside is recycled. The test section of the wind tunnel has a cross-section (height by width) of 1.23 by 1.52 m, and an undisturbed horizontal section of roughly 5 to 6 m which may be used for probing. During the experiment two segments of one cable (which encloses the ~~FOs~~FO cores) were placed 8 cm apart: one heated and one reference segment. For validation, an independent sonic anemometer (IRGASON+EC100 and CR3000, Campbell Scientific, Logan, UT,USA) was placed approximately 0.2 m downwind of the fibers, which measures the wind speed in 3 directions ~~.~~at 10 Hz. As the FO cables are very thin, it is assumed that these do not significantly disturb the measurement of the sonic volume (particularly at larger averaging times). All equipment was mounted using custom-designed support material.

The ~~angle of the fiber related to the flow, wind speed and heating rate were systematically changed. An electrical current (I) is passed through the heated cable, to create the temperature difference that is necessary to measure wind speed (ΔT, e.g., 2 K) . By fixing the current through the stainless steel casing~~ cable (AFL, Spartanburg, SC, USA) mounted in the wind tunnel consisted of a 1.34 mm outer diameter stainless steel casing that enclosed four multi-mode FO cores with a diameter of 250 µm (Figure A1). The electrical resistance per meter of stainless steel casing (R_s) is 1.67 ($\Omega\mathrm{m}^{-1}$) and is constant along the length, where for the length of a cable segment (B, (m)), $R = R_sB$, where R (Ω) is the total resistance of a cable segment. Similary the heating rate is defined as $P_s = I^2R_s$ (Wm^{-1}) per meter of cable segment, where I (A) is the eletrical current. Only two FO cores were used and these were spliced at the end of the cable ~~, the entire FO cableis heated because of the electrical resistance (R)of the~~ to create a duplexed FO core, which results in double measurements for each measuring point along the FO cable, using a single-ended configuration (Hausner et al., 2011). The FO cores were connected to a Silixa Ultima DTS machine (Ultima S, 2 km range, Silixa, London, UK) outside the wind tunnel.

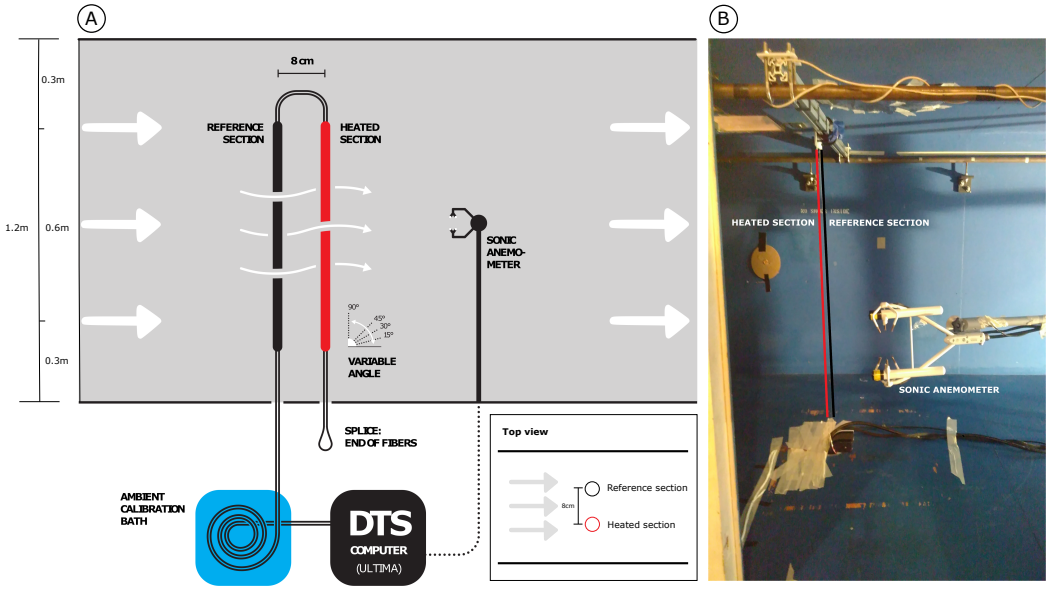

Figure 2. a) Schematic of the wind tunnel setup and b) photograph of the experimental setup in the wind tunnel.

One cable segment was heated by connecting the stainless steel casing ~~. The magnitude of the current needed to create a given temperature difference is dependent on the cable resistance and the wind speed, therefore the current is adjusted for each individual experiment. The amount of power applied per meter of cable, P_s (W~~m to a power controller (MicroFUSION uF1HXTA0-32-P1000-F040) by 12 AWG (copper) cables (3.31 mm^2), to heat the cable in a controlled way.

For calibration and validation of the DTS data, approximately 6 m of the FO cables was placed in a well-mixed ambient bath to calibrate the DTS temperature according to the method described by Hausner et al. (2011). The temperature was verified with one probe (RBRsolo~~$^{-1}$), necessary to heat the cable and to create a temperature difference, is referred to as the heating rate.~~^{2} T, RBR Ltd., Ottawa, Ontario, Canada). A circulating aquarium pump was placed inside the bath, to prevent stratification.

In field experiments the wind speed and direction will vary, therefore different angles of attack and wind speeds are tested. Additionally different heating rates are used to quantify the importance of the signal-to-noise ratio. The following settings are used:

- **Angle of attack**: The cable was mounted at four different angles in the wind tunnel, resulting in different angles of attack to mean flow direction, in order to gain more insights into directional sensitivity. In Figure 2b the 90° set-up is visible, however the cable was also mounted at a 45°, 30° and 15° angle, with respect to the floor of the wind tunnel (see: Figure 2a, inset). During all set-ups, the lower part of the FO cable was fixed to the opening in the bottom of the wind tunnel, while the upper end was attached to an extruded aluminum bar that was moved over the fixed horizontal bars, to achieve the desired cable angles.

- **Wind speed**: To test the performance for a range of wind speeds, ten different wind speeds were tested at every angle: 1, 3, 5, 7, 9, 11, 13, 15, 16 and 17 ms^{-1} ~~(e. g., 4x10 = 40 setups).~~ . The AHFO wind speed measurements can be ~~calibrated~~ adjusted by comparing the AHFO wind speed to a reference sonic anemometer. The wind speed in the wind tunnel was fixed at a constant value to create a stable, non-turbulent, steady state flow (Appendix C). ~~In field experiments the wind speed will vary, and the temperature difference will fluctuate accordingly if the current is fixed. In order to quantify the importance of the signal-to-noise ratio for all possible combinations of angles and wind speed (4 x 10), three temperature differences were applied~~

- **Heating rate**: The magnitude of the current needed to create a given temperature difference is dependent on the cable resistance and the wind speed, therefore the current is adjusted for each individual experiment. The current was fixed to create a temperature difference (ΔT) of 2, 4 and 6 K between the heated and reference cable. Heating rates varied from 0.5-10 Wm^{-1} during our setup.

In total, 120 (4 x 10 x 3) trials were conducted with the different parameters, each with a minimum duration of 10 minutes.

~~The cable mounted in the wind tunnel consisted of a 1.34 mm outer diameter stainless steel casing that enclosed four multi-mode FOs with a diameter of 250 µm (Figure A1). Only two FOs were used and these were spliced at the end of the cable to create a duplexed FO, which results in double measurements for each measuring point~~ Temperatures along the FO ~~(Hausner et al., 2011). The FOs were connected to a Silixa Ultima DTS machine (Ultima S, 2 km range, Silixa, London, UK) outside the wind tunnel.~~

~~Cross-section of the FO cable~~

~~One cable segment was heated by connecting the stainless steel casing to a power controller (MicroFUSION uF1HXTA0-32-P1000-F040) by 12 AWG (copper) cables (3.31 mm^2), to heat the cable in a controlled way. Heating rates varying from 0.5-10 Wm^{-1} were used to create temperature differences to a fixed level depending on the setup. The electrical resistance per meter of stainless steel casing (R_s) is 1.67 (Ωm^{-1}) and is constant along the length. For the length of a cable segment (B, (m)), $R = R_s B$, where R (Ω) is the total resistance of a cable segment. The same holds for $P = P_s B$, where P (W) is the total power input for a cable segment. The heating rate for a cable segment (Wm^{-1}) was controlled by fixing the current, I (A), during experiments, as the current is also constant over the entire heated segment, the heating rate is as well. Hence, the known relation $P = I^2 R$ (W), or in this specific case the heating rate is $P_s = I^2 R_s$ (Wm^{-1}) per meter of cable segment.~~

~~For calibration and validation of the DTS data, approximately 6 m of the FO cables was placed in a well-mixed ambient bath to calibrate the DTS temperature according to the method described by Hausner et al. (2011). The temperature was verified with one probe (RBRsolo^2 T, RBR Ltd., Ottawa, Ontario, Canada). A circulating aquarium pump was placed inside the bath, to prevent stratification.~~

~~Temperatures along the FOs were~~ cable were sampled at 0.125 m resolution with a sampling rate of 1 Hz. ~~The FOs were deployed in a double-ended configuration, however the data was acquired and treated as two separated single-ended channels of data.~~ Splices between ends of fiber optic cables are known to create an additional loss in signal, i.e., local higher attenuation (Tyler et al. (2009); van de Giesen et al. (2012)), this loss is normally independent of the direction. However, in processing

of the raw DTS data it was found that the loss over the splice was not the same in both directions. Due to this asymmetrical structure of the splice loss, only the data of one channel was used to ensure the quality of the results, as this channel showed a regular splice loss.

For each angle of attack only the 5 temperatures differences ($\times 2$ because of duplexing) from the middle of the wind tunnel are used, to prevent using AHFO wind speed measurements with side/boundary effects. We investigated the consequences of extending the spatial range and found there is limited difference between these measurements (see Table D1). During this extended spatial range analysis we found out part of the 90° data of the duplexed cable contained additional noise which decreased the accuracy, and therefore we decided to take only 5×1 temperature differences for the 90° calculations.

In our study we use the advantage of averaging over time and space, to reduce (white) noise in the DTS measurements (van de Giesen et al. (2012); Selker et al. (2006b)). For clarity we therefore introduce three parameters: n_{time}, n_{space} and n, where n_{time} is the amount of measurements averaged over time and n_{space} is the amount of measurements averaged over space and n the total amount of measurements over time and space and can be expressed as: $n = n_{time} \times n_{space}$. In the machine specifications it is given that the sample resolution is $x_{sample} = 0.125$m, but the highest actual spatial resolution is 0.3m, indicating and $n_{space} \geq 2$. In this paper we will first work with $n_{space} = 10$ and finally we will propose an equation (See later Eq. 21) which is a function of ~~$n_{space} = 1$~~ n_{space} and n_{time}. This is done, because we want to estimate an unique constant (C_{DTS}) independent of the DTS machine and the settings, which is expected to be more representative if the amount of (white) noise is reduced by averaging.

~~To be able to test the accuracy of the DTS wind speed measurements independently, wind speed was sampled at 10 Hz using a sonic anemometer (IRGASON+EC100 and CR3000, Campbell Scientific, Logan, UT,USA). The sonic anemometer was mounted approximately 0.2 m behind the fiber optic cables, in the middle of the wind tunnel. As the FOs are very thin, it is assumed that these do not significantly disturb the measurement of the sonic volume (particularly at larger averaging times).~~

2.4 Directional sensitivity analysis

Equation 10 is derived for flows normal to axis of the cable (as in Figure 2b). However, in reality the wind will not always have a 90° angle compared to the axis of the cable, especially in outside atmospheric experiments. For angles smaller than 90° the wind speed will be underestimated, as the ~~advective~~ convective heat transfer is less efficient. ~~To be able to still determine the wind speed for all angles of attack,~~ While Sayde et al. (2015) adjusted the wind speed ~~obtained in Eq. 10~~ of the sonic anemometer using a geometric correction from hotwire anemometry (e.g., Adrian et al. (1984))~~to get the true wind speed (u_{DTS})~~, we adjusted the measured DTS windspeed u_N (eq. 10) to compare both wind speeds:

$$u_{DTS} = \sqrt{\frac{u_N^2}{\cos^2(\varphi - 90°) + k_{ds}^2 \sin^2(\varphi - 90°)}} \tag{11}$$

k_{ds} is the directional sensitivity and φ is the angle of attack of the wind with respect to the axis of the cable, ranging from 0° to 90°.

2.5 Accuracy and precision definition

The perfomance of our AHFO measurements will be assed by looking at the accuracy and precision. The accuracy (σ_a) is defined by the normalized difference of the AHFO and sonic anemometer wind speed measurements, Eq. 12.

$$\sigma_a(j) = \frac{\bar{u}_{DTS}(j) - \bar{u}_{sonic}(j)}{\bar{u}_{sonic}(j)} \tag{12}$$

Where j is a specific wind speed setting, where $j = 1,3,5,7,9,11,13,15,16,17$ ms^{-1}. And $\bar{u}$ is the average of all indivual measurements (i) for a given wind speed setting.

The precision (σ_p) is defined by the normalized RMSD between the AHFO and sonic anemometer wind speed measurements, 13.

$$\sigma_p(j) = \frac{\text{RMSD}}{\bar{u}_{sonic}(j)} = \frac{\sqrt{\sum \left(\left(u_{sonic}(i,j) - \bar{u}_{sonic}(j) \right) - \left(u_{DTS}(i,j) - \bar{u}_{DTS}(j) \right) \right)^2 \frac{1}{n(i)}}}{\bar{u}_{sonic}(j)} \tag{13}$$

3 Results and Discussion

3.1 Proposed directional sensitivity equation

During analysis of the wind tunnel data it was found that Eq. 11 was not giving satisfying results (e.g., a 22% bias between the 90° and 15° angle). In Adrian et al. (1984) it is shown that in hotwire anemometry a variety of theoretical and empirical formulas have been proposed in the past, in order to account for directional sensitivity. Alternatively, using the formula suggested by Bruun (1971) gives more satisfying results, diminishing the bias between the 90° and 15° angle to only 4%. This is shown in the boxplot of Figure 3.

Therefore, Eq. 14 is used to account for directional sensitivity in our study, with the scaling exponent, m_1, able to be optimized during calibration of the AHFO measurements. The value for m_1 obtained during calibration of our set up was 1.05.

$$u_{DTS} = \frac{u_N}{\cos(\varphi - 90°)^{m_1}} \tag{14}$$

3.2 Accuracy and precision

In Figure 3b the AHFO wind speed measurements are compared to the velocity measured with the sonic anemometer. The comparison for all angles can be found in Figures B1 and B2. The wind speeds measured with AHFO are calculated using 10 temperature differences (duplex setup with 2×5 heated and reference measurements), i.e., for the 90°setup this is equivalent

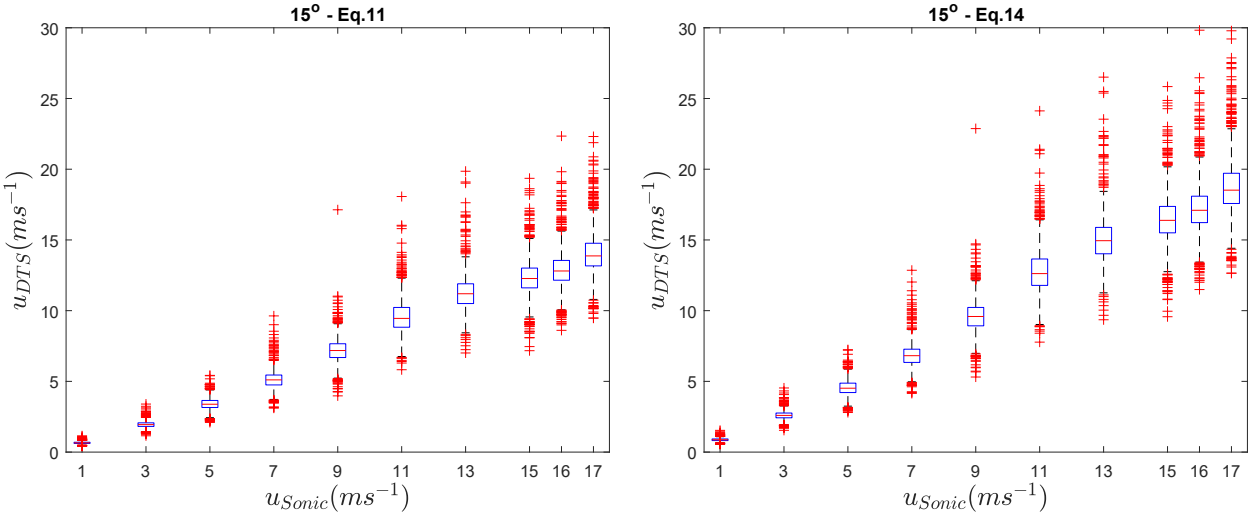

Figure 3. Directional sensitivity shown in boxplots for 15° angle, original Eq. 11 (a) and proposed Eq. 14 (b).

to a height of $\sim$ 0.675 m in the wind tunnel. ~~For each angle of attack only the 5 temperatures differences ($\times$2 because of duplexing) from the middle of the wind tunnel are used, to prevent using AHFO wind speed measurements with side/boundary effects. We investigated the consequences of extending the spatial range and found there is limited difference between these measurements (see Table D1). During this extended spatial range analysis we found out part of the 90° data of the duplexed cable contained additional noise which decreased the accuracy, and therefore we decided to take only 5 $\times$ 1 temperature differences for the 90° calculations.~~

Figure B1 shows the ~~1 s~~ sample rate DTS data against the ~~1 s~~ 1-s average sonic anemometer data, for the four different angles of attack. Figure B2 shows the same dataset, but temporally averaged over ~~30 s~~30-s, and for all angles. A clear improvement of the precision is visible when temporal averaging is performed. Even though the directional sensitivity formula is not yet fully calibrated, the bias is negligible, with coefficients of determination ranging from ~~0.85-0.98~~0.94-0.99. Finally, as expected, the wind speed measurement are less accurate when the wind speed angle is smaller.

To get more insight in the quality of the results, a dimensionless analysis is performed. In Figure 4, the non-dimensional wind speed accuracy for the whole wind tunnel experiment is shown. For all combinations (120 individual cases of varying wind speed (~~u_j~~ j), angle and ΔT), the accuracy is calculated according to Eq. 12. σ_a is a ~~function of~~ dependent on the averaging time, which is defined as $n_{time} = t_{avg}/t_{sample}$, where t_{avg} can only be a integer which is a multiple of t_{sample}. σ_a is also a ~~function of~~ dependent on spatial averaging, which is defined as $n_{space} = x_{avg}/x_{sample}$, where x_{avg} can only be a integer which is a multiple of x_{sample}. In Figure 4 the accuracy is averaged over all wind speeds for each ΔT and angle combination, with $n_{space} = 10$ and n_{time} varying from 1 to 30, resulting in 12 values for each time resolution~~, which can be written as: $\sigma_a(\bar{u}_j, n_{space} = 10, n_{time} = 1,5,10,15,20,25,30)$. Where $\bar{u}_j$ is the average over all individual measurements (i) of a specific wind speed u_j , where $j = 1 - 17 ms^{-1}$~~.

$$\sigma_a(u_j, n_{space}, n_{time}) = \frac{\bar{u}_{DTS}(j) - \bar{u}_{sonic}(j)}{\bar{u}_{sonic}(j)}$$

For the data set, the maximum σ_a is $\pm$ 3%, which is promising for future applications. The $\Delta T = 6K$ should be the best performing heating setting, however this is not always the case and there is fluctuations between the heating settings, which could be due to neglecting small energy losses, like free convection due to heating of air close to the heated cable (Sayde et al. (2015)), which is temperature dependent. With such an energy loss included, the bias of each angle might change. Nevertheless, the bias is fairly constant with increasing averaging time, which means extensive calibration can probably increase the accuracy.

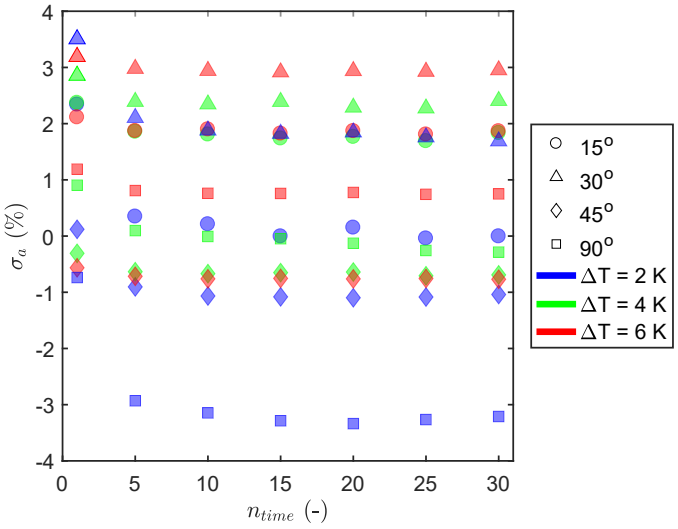

Figure 4. Bias in AHFO wind speed as a function of averaging period for different angles of attack, and different fiber heating. With $n_{space} = 10$.

While the accuracy (bias) remains constant over the averaging period, the relative precision, σ_p improves significantly (Fig. 5). The precision is calculated for all 120 ΔT, angle and wind speed combinations (~~u_j, where $j = 1 - 17 ms^{-1}$~~)where $j = 1, 3, 5, 7, 9, 11, 13, 15, 16, 17$ ms^{-1}), using Eq. 13.

$$\sigma_p(u_j, n_{space}, n_{time}) = \frac{\text{RMSD}}{\bar{u}_j} = \frac{\sqrt{\sum \left(\left(u_{sonic}(i,j) - \bar{u}_{sonic}(j) \right) - \left(u_{DTS}(i,j) - \bar{u}_{DTS}(j) \right) \right)^2 \frac{1}{n(i)}}}{\bar{u}_{sonic}(j)}$$

Similar to the accuracy, the precision, σ_p, is ~~a function of~~ dependent on the averaging time ~~, which is again defined as $n_{time} = t_{avg}/t_{sample}$, where t_{avg} can only be a integer which is a multiple of t_{sample}. The precision, σ_p is also a function of spatial averaging, which is also here defined as $n_{space} = x_{avg}/x_{sample}$, where x_{avg} can only be a integer which is a multiple of x_{sample}~~and spatial averaging.

While calculating the precision of u_{DTS}, the natural variability of the wind is excluded, by assuming the sonic anemometer is able to capture the natural variability and assuming the sonic anemometer measurements have a negligible instrument variability in comparison to the AHFO measurements. As a result, the variability of the DTS machine u_{DTS} estimates are obtained. For each of the 120 combinations, $\bar{u}_{sonic}(j)$ and $\bar{u}_{DTS}(j)$ are the average wind speeds for ~~an u_j~~ a j. $u_{sonic}(i,j)$ and $u_{DTS}(i,j)$ are single measurements for ~~an u_j~~ a j.

To be able to present the precision clearly, the precision is averaged over wind speed for all ΔT and angle combinations in Figure 5, with n_{space}=10 and n_{time} varying from 1 to 30, resulting in 12 values for each time resolution~~, which can be written as Eq. ??, with $n_{space} = 10$ and $n_{time} = 1, 5, 10, 15, 20, 25, 30$:~~

$\sigma_p = f(\bar{u}_j, n_{space}, n_{time})$

.

The precision improves to a σ_p less than 5% by averaging over time. Improvement by averaging is expected due to the reduction of noise (van de Giesen et al. (2012)). As mentioned, the main source of noise in DTS data is white noise, this explains the visible improvement of the precision by $\frac{1}{\sqrt{n}}$, as signal averaging is applied, where n is the amount of measurements (Selker et al. (2006b); Kaiser and Knight (1979)). Hence, in this paper n is expressed as $n_{space} \times n_{time}$, the amount of measurements in the time and space domain.

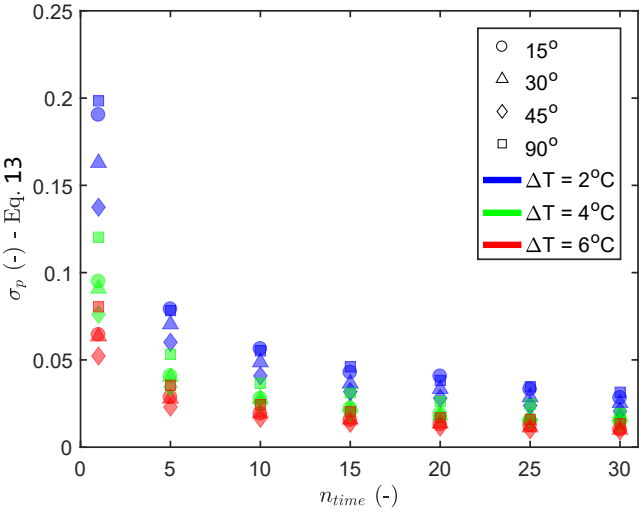

Figure 5. Precision of the AHFO wind speed measurements as a function of averaging period. With $n_{space} = 10$.

3.3 Normalized precision independent of sampling settings

In order to remove the influence of different settings (such as the choice of ΔT) and determine a general prediction of precision in future experiments, we normalize the precision. First, the precision is normalized to ΔT (Figure 6a), by multiplying Eq. ~~??~~

13 by $\frac{\Delta T}{T_{error}}$, which can be written as Eq. 15.

$$\sigma_p = f_p(j, n_{space}, n_{time}\Delta T) = \sigma_p(j) \cdot \frac{\Delta T}{T_{error}} \tag{15}$$

As a results, $\frac{1}{\sqrt{n}}$ dependence becomes even more clear, as shown by the black solid line showing $\frac{\bar{\sigma}_p}{\sqrt{n_{time}}} \times \frac{\Delta T}{T_{error}}$, where $\bar{\sigma}_p$ is the average of Eq.??13, with $n_{space} = 10$ and n_{time}=1. Second, the precision is also normalized to the $\frac{1}{\sqrt{n}}$ behavior, by multiplying Eq. 15 by $\sqrt{\frac{t_{avg}}{t_{sample}}}$, resulting in Eq. 16.

$$\sigma_p = f_p(j, n_{space}\Delta T, n_{time}) = \sigma_p(j) \cdot \frac{\Delta T}{T_{error}} \sqrt{\frac{t_{avg}}{t_{sample}}} \tag{16}$$

T_{error} and t_{sample} are given constants which depend on the performance of the DTS, in this case $T_{error} = 0.25$ K and $t_{sample} =$ ~~1 s~~1-s, according to the factory specifications. It appears that the precision by taking the average can be condensed in one number, 1.6, which we denote by the symbol C_{int} (Figure 6b). Intermediate constant C_{int} can be defined as, Eq. 17, with $n_{space} = 10$:

$$C_{int} = \overline{\sigma_p(j) \cdot \frac{\Delta T}{T_{error}} \sqrt{n_{time}}} = 1.6 \tag{17}$$

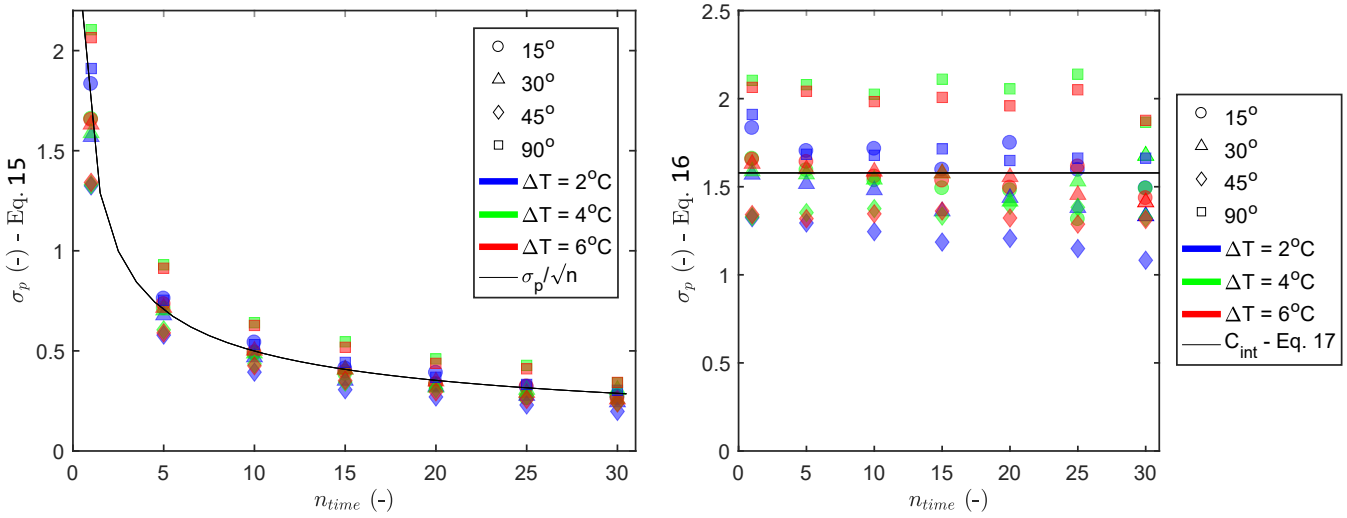

Figure 6. a) Precision of the AHFO wind speed measurements as a function of averaging period, independent of ΔT; and b) Precision of the AHFO wind speed measurements as a function of averaging period. Independent of ΔT and averaging period. With $n_{space} = 10$.

Finally, a final constant for a ~~1 s~~1-s and 0.125~~m~~-m resolution is desired, as this is the sampling resolution and the starting point before any averaging takes place. Doing so, Eq. 21 can be used for different kinds of DTS machines, also when a DTS machine has different sampling resolutions. Furthermore it is possible to increase the precision of the observation by either

averaging over space or time, depending on the scientific research question to be answered with AHFO. By using the shown $\frac{1}{\sqrt{n}}$ dependency, we can convert C_{int} into C_{DTS}, by multiplying C_{int} by $\sqrt{\frac{10}{1}}$, as n_{space} is 10. This results in Eq. 18 with n_{space}=1 and n_{time}=1. C_{DTS} is in our paper on purpose not calculated at once, but derived using C_{int}. As the wind speed in the middle of the wind tunnel can be assumed constant, we expect C_{DTS} to be better by using 5 measurements in the middle of the wind tunnel instead of picking one of these 5.

$$C_{DTS} = \overline{\sigma_p(j) \cdot \frac{\Delta T}{T_{error}} \sqrt{n_{time}}} \cdot \sqrt{n_{space}} = C_{int}\sqrt{10} = 5.0 \tag{18}$$

3.4 Precision prediction

At the start of a new AHFO experiment it is unknown how to make sure the signal-to-noise ratio is sufficient, such that σ_p is small. However, given the result that the increase in precision behaves independent of ΔT and the averaging time, it is possible to make a prediction for the precision of future work.

In outdoor experiments, the only setting which can be changed is the heating rate, P_s, which is assumed to be fixed at a single value. The idea behind the precision prediction is to guide the choice of a heating rate, such that a preferred precision is achieved for a known dominant wind speed range. As the wind speed outside will vary naturally, ΔT will change accordingly. Therefore, to obtain an expression where P_s is the only unknown, ΔT first needs to be expressed as a function of the wind speed u_n and the heating rate (P_s). This can be done by using Eq. 10. To obtain a first estimate, some assumptions can be made. The numerator of Eq. 10 consists of three terms, of which the first one with heating rate (P_s) is dominant compared to the other ones, namely 10-100 times bigger. When these minor terms are neglected Eq. 10 can be simplified to:

$$u_N = \left(\frac{0.5 P_s \pi^{-1} r^{-1}}{C d^{m-1} \mathrm{Pr}^n K_a \upsilon_a^{-m} (T_s - T_f)} \right)^{1/m} = \left(\frac{A P_s}{B \Delta T} \right)^{1/m} \tag{19}$$

With $A = 0.5\pi^{-1}r^{-1}$, $B = C(d)^{m-1}\mathrm{Pr}^n K_a \upsilon_a^{-m}$ and $\Delta T = T_s - T_f$, resulting in an expression for ΔT as a function of wind speed:

$$\Delta T = \frac{A P_s}{B u_n^m} \tag{20}$$

Knowing this expression of ΔT, Eq. 20 can again be rewritten into Eq. 21, which expresses the precision estimate, with P_s as only parameter which can be changed during an experiment.

$$\sigma_p(u_j j, n_{space}, n_{time}, P_s) = C_{DTS} \frac{B T_{error} u_n^m}{A P_s} \sqrt{\frac{1}{n_{space} \cdot n_{time}}} \tag{21}$$

Where $n_{space} \times n_{time}$ is the number of measurements over which the observed wind speed is averaged, in either space or time domain. By assuming that all constants are known from literature and the set-up, a first estimate of the error can be made

for every velocity or heating rate given. If a dominant wind speed range for a new project is known, an associated heating rate can be found, such that the error is sufficiently small.

As an example, Figure 7 shows the estimated precision for our experiment at ~~1 s~~ 1-s ($n_{time} = 1$) and ~ 0.675~~m~~ -m ($n_{space} = 10$) resolution over a range of wind speeds and heating rates. If the diameter of the fiber is different, this is taken into account via term A from Eq. 21, which includes the radius ($d = 2r$). Also, when a DTS machine with a different performance is used, this can be implemented by changing T_{error} accordingly. Of course different applications will demand different space-time averaging windows, depending on the scientific research question to be answered with AHFO, which option is included by $\sqrt{\frac{1}{n_{space} \cdot n_{time}}}$.

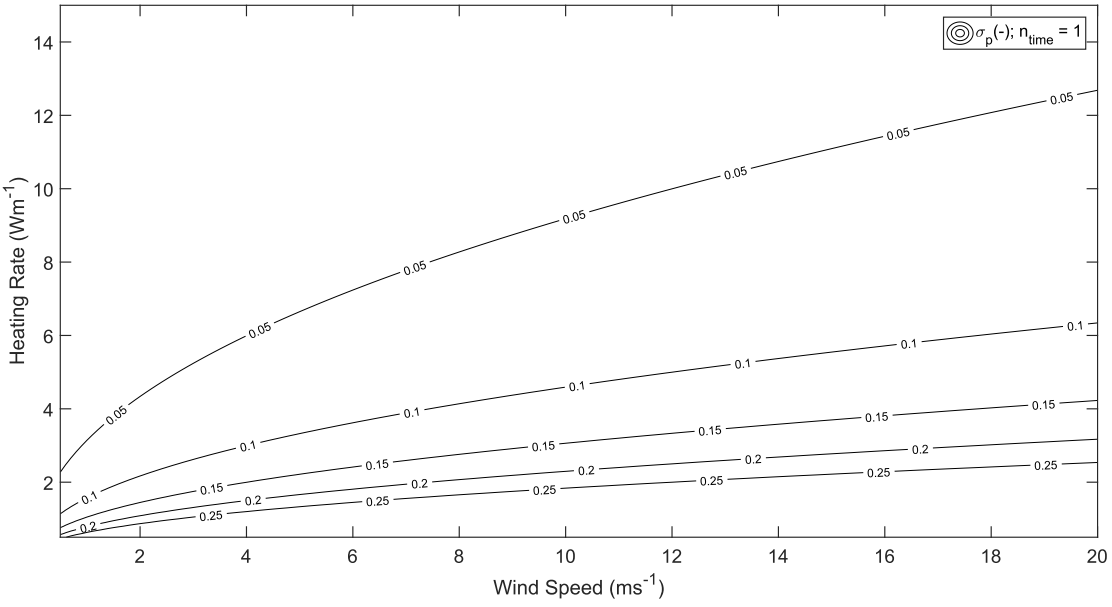

Figure 7. Expected precision (contour lines) for a given heating rate and wind speed as calculated from Eq. 21, with $n_{space} = 10$ and $n_{time} = 1$.

In outdoor experiments, the influence of the short and long wave radiation will be present. However, as long as the radiation is the same for the heated and non-heated segment, this does not influence the error estimation, as for the signal-to-noise ratio, ΔT is the most important factor. When the heated and reference fiber are close to each other, which is also needed for properly estimating the wind speed, both fibers will experience a similar contribution of external radiation, such that the overall ΔT will be relatively unaffected by this factor.

3.5 Considerations using AHFO outdoors

The experiments described here were performed in a controlled wind tunnel environment. When performing outdoor AHFO experiments, several factors need to be considered. First of all, during field experiments the relative humidity and temperature might have such a big range that assuming certain parameters (e.g., K_a and υ_a) as constant is not applicable anymore (Tsilingiris (2008)). Furthermore, for small wind speeds (e.g., < 1 ms^{-1}), the neglection of energy losses like free convection seems not entirely applicable, as this term becomes more dominant in comparison to forced convection. This is confirmed in our study, where it was visible that the response is different between a well ventilated and non-ventilated cable, hence the accuracy is dependent on the wind speed. Although not shown in this paper, it seemed there was no time response difference between a vertical or horizontal mounted heated cable, however by mounting the cable in a horizontal or vertical direction, free convection might influence the temperature measurements as the heated air is moving upward.

Also, the flow in the wind tunnel is laminar and has less turbulence than in outdoor conditions (Appendix C). This is a good setting for calibration of the AHFO method, however in outdoor conditions (small scale) turbulence around the cable is something to take into account. Especially with smaller wind speeds the cooling by turbulence around the cable can be an additional heat loss component, which is not included in the energy balance and therefore could lead to overestimation of the wind speed.

It is shown that AHFO can give reliable wind speed measurements, however the precision and accuracy is not as good as with a sonic anemometer. The major addition of AHFO is the possibility to sample the wind speed with a high spatial distribution. It should be taken into account that the time resolution is lower than that of a sonic anemometer and therefore AHFO is less suitable for small scale turbulence, but ~~turbulence~~ larger scale turbulence (>1-s; >0.3-m) can potentially be fully captured ~~due to the~~ with a 2D/3D setup with distributed measurements. Despite the high potential resolutions (~~1s~~ 1-s and 0.3~~mm~~-m) the user should consider to average in either the space or time domain to enhance the precision of the obtained data. The choice for averaging over space or time should be made based on the researched topic.

Finally, when measuring in the field, the use of high quality reference point measurements (e.g., sonic anemometer) is recommended, for example to be able to compensate for possible biases. A sonic anemometer can also be useful to determine the angle of attack, as this is not (yet) possible with one single fiber. A more complex 3D set-up is necessary to be able to do this with DTS/AHFO (Zeeman et al. (2015)), something which would be interesting to be tested with AHFO in a field experiment.

4 Conclusions

Through a series of controlled wind tunnel experiments, new insights into the accuracy and precision of the newly introduced AHFO wind speed measuring technique were obtained. With high spatial (0.3~~m~~-m) and temporal (~~1 s~~1-s) resolution, the AHFO wind speed measurements agreed very well with the sonic anemometer measurements, with a coefficients of determination ranging from 0.94-0.99. It is also shown that the AHFO technique has the possibility to measure with a precision and accuracy of 95%. Some additional work is needed, as there still is a small overestimation, which may be caused by neglecting some

energy fluxes, such as free convection due to heating of the air close the heated cable. Furthermore, it is possible to optimize the directional sensitivity compensation by extended calibration.

The error prediction equation (Eq. 21) is an important result of this work that will aid in the design of future experiments. This design tool helps with choosing a heating rate for the actively heated fiber in order to be able to create a sufficiently high precision. Based on the prevalent wind speeds of a potential field experiment site, a first estimate of an associated sufficient heating rate can be calculated. Due to the way this design tool is constructed, it can be ~~generalized~~ a good first estimate for all kinds of fibers, DTS precisions, and user preferred spatial and temporal resolutions.

The AHFO technique can reliably measure wind speeds under a range of conditions. The combination of high spatial and temporal resolution with high precision of the technique opens possibilities for outdoor application, as the key feature of the AHFO is the ability to measure spatial structures in the flow, over scales ranging from one meter to several kilometers. In the future, the technique could be useful for micrometeorological and hydrological applications~~in complex terrain~~, allowing for characterization of spatial varying fields of mean wind speed, such as in canopy flows or in sloping terrain.

Author contributions. Justus van Ramshorst prepared and performed the experiments, worked on analyzing the data and writing the manuscript. John Selker and Chad Higgins assisted with the experiments and analyzing the data and contributed to the manuscript. Miriam Coenders-Gerrits, Bart Schilperoort, Bas van de Wiel and Jonathan Izett helped with analyzing the data and contributed to the manuscript. Huub Savenije and Nick van de Giesen contributed to the manuscript.

Competing interests. The authors declare that they have no conflict of interest.

Acknowledgements. Many thanks for the practical assistance of Cara Walter and Jim Wagner with the AHFO/DTS setup and appreciation for the people of the OPEnS LAB for assisting with the assembling of parts. This project was partly funded by NWO Earth and Life Sciences, Veni project 863.15.022, The Netherlands. We are also grateful for the funding by Holland Scholarship and CTEMPs.

Appendix A: ~~Comparison of AHFO and sonic anemometer wind speed~~

Appendix A: FO cable schematization

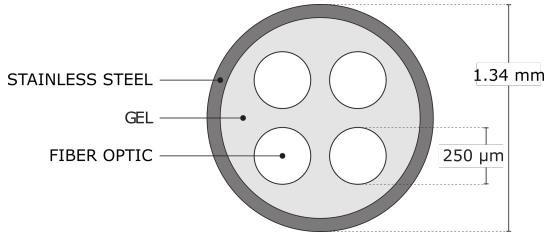

Figure A1. Cross-section of the FO cable

Appendix B: Comparison of AHFO and sonic anemometer wind speed

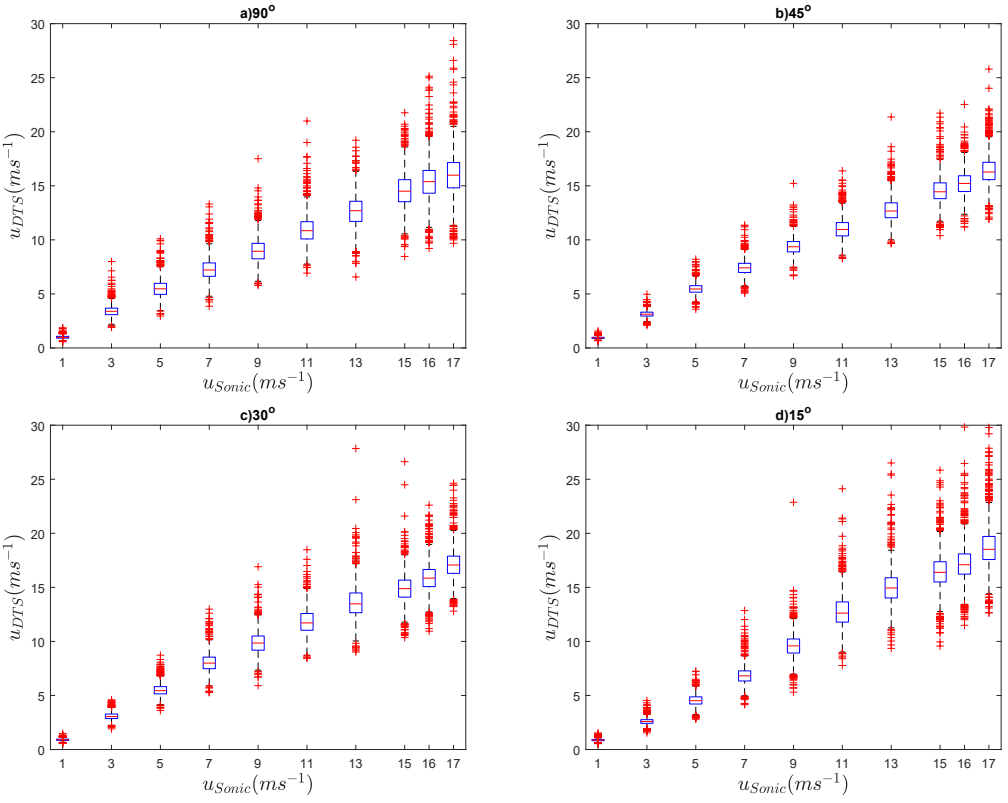

Figure B1. Comparison of AHFO and sonic anemometer wind speed at a ~~1 s~~ 1-s temporal resolution, for the four different angles of attack. a) 90°, b) 45°, c) 30°, and d) 15°. $n_{space} = 10, n_{time} = 1$.

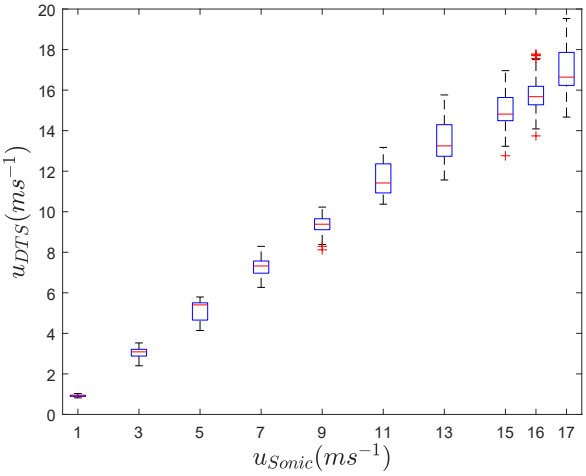

Figure B2. Comparison of AHFO and sonic anemometer wind speed averaged over 30 s~~for~~. The boxplot includes the measurements of all angles of attack. $n_{space} = 10, n_{time} = 30$.

Appendix C: Wind tunnel flow characteristics

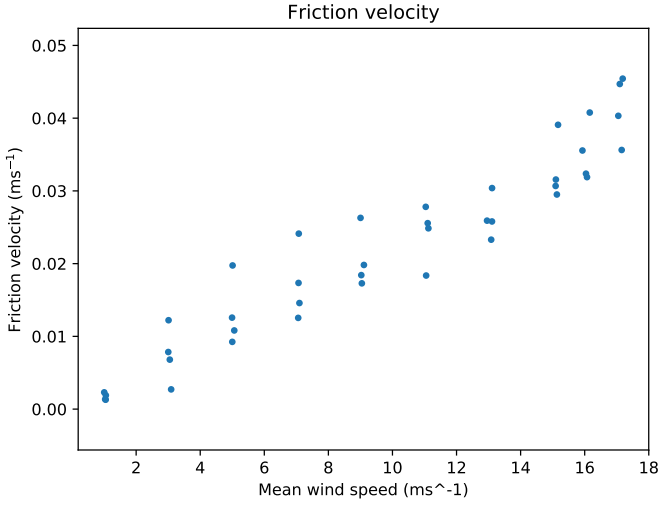

Figure C1. Friction velocity (ms^{-1}) in the wind tunnel during AHFO experiment.

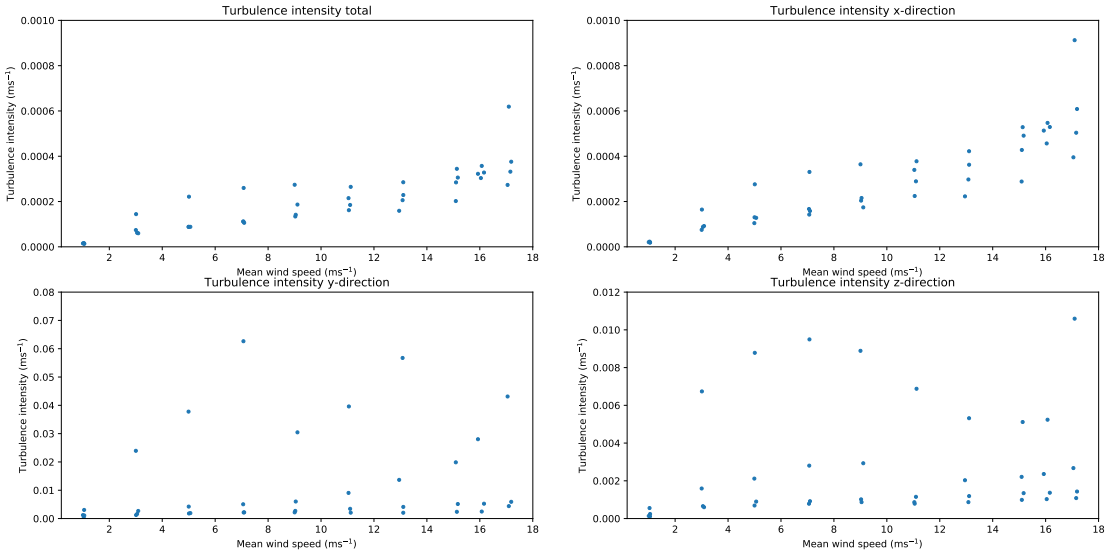

Figure C2. Turbulence intensity (variance devided by mean wind speed) (ms^{-1}) in the wind tunnel during AHFO experiment. The x-direction is in the flow direction. The y-direction is the width direction. The z-direction is the height direction.

Table D1. Standard deviation σ_{space} of 5 pairs of AHFO measurements (duplex configuration) per wind speed, and its normalized standard deviation. It shows that the normalized standard deviation is $\approx 3\%$ no matter if one takes the top, mid-top, center, mid-bottom, or bottom pair.

u (ms^{-1})	1	3	5	7	9	11	13	15	16	17
σ_{space} (ms^{-1})	0.033	0.092	0.147	0.181	0.235	0.312	0.323	0.445	0.526	0.544
Normalized σ_{space} (%)	0.033	0.031	0.029	0.026	0.026	0.028	0.025	0.030	0.033	0.032

For each angle and power rate, the u_{dts} was calculated with only the two temperature differences (duplex configuration) of the top of wind tunnel, or the mid-top, center, mid-bottom, or bottom of the wind tunnel (thus $n_{space} = 2$). From these 5 pairs we calculated the standard deviation σ_{space} per wind speed.

Appendix D: Extended spatial range

References

Adrian, R. J., Johnson, R. E., Jones, B. G., Merati, P., and Tung, A. T.: Aerodynamic disturbances of hot-wire probes and directional sensitivity, Journal of Physics E: Scientific Instruments, 17, 62–71, https://doi.org/10.1088/0022-3735/17/1/012, 1984.

Baldwin, A. J. and Lovell-Smith, J. E. R.: The emissivity of stainless steel in dairy plant thermal design, Journal of Food Engineering, 17, 281–289, https://doi.org/10.1016/0260-8774(92)90045-8, 1992.

Bentamy, A., Katsaros, K. B., Mestas-Nuñez, A. M., Drennan, W. M., Forde, E. B., and Roquet, H.: Satellite Estimates of Wind Speed and Latent Heat Flux over the Global Oceans, Journal of Climate, 16, 637–656, https://doi.org/10.1175/1520-0442(2003)016<0637:SEOWSA>2.0.CO;2, 2003.

Bou-Zeid, E., HIGGINS, C., HUWALD, H., MENEVEAU, C., and PARLANGE, M. B.: Field study of the dynamics and modelling of subgrid-scale turbulence in a stable atmospheric surface layer over a glacier, Journal of Fluid Mechanics, 665, 480–515, https://doi.org/10.1017/S0022112010004015, http://www.journals.cambridge.org/abstract{_}S0022112010004015, 2010.

Bruun, H. H.: Interpretation of a Hot Wire Signal Using a Universal Calibration Law., Journal of Physics E: Scientific Instruments, 4, 225–231, https://doi.org/10.1088/0022-3735/4/3/016, 1971.

Cengel, Y. and Ghajar, A.: Heat and mass transfer: fundamentals and applications, McGraw-Hill Higher Education, 2014.

Euser, T., Luxemburg, W. M. J., Everson, C. S., Mengistu, M. G., Clulow, A. D., and Bastiaanssen, W. G. M.: A new method to measure Bowen ratios using high-resolution vertical dry and wet bulb temperature profiles, Hydrology and Earth System Sciences, 18, 2021–2032, https://doi.org/10.5194/hess-18-2021-2014, 2014.

Goodberlet, M. A., Swift, C. T., and Wilkerson, J. C.: Remote sensing of ocean surface winds with the special sensor microwave/imager, Journal of Geophysical Research, 94, 14 547–14 555, https://doi.org/10.1029/JC094iC10p14547, 1989.

Ha, K.-J., Hyun, Y.-K., Oh, H.-M., Kim, K.-E., and Mahrt, L.: Evaluation of Boundary Layer Similarity Theory for Stable Conditions in CASES-99, Monthly Weather Review, 135, 3474–3483, https://doi.org/10.1175/MWR3488.1, http://journals.ametsoc.org/doi/abs/10.1175/MWR3488.1, 2007.

Hausner, M. B., Suárez, F., Glander, K. E., van de Giesen, N., Selker, J. S., and Tyler, S. W.: Calibrating single-ended fiber-optic raman spectra distributed temperature sensing data, Sensors, 11, 10 859–10 879, https://doi.org/10.3390/s111110859, 2011.

Higgins, C. W., Meneveau, C., and Parlange, M. B.: Geometric Alignments of the Subgrid-Scale Force in the Atmospheric Boundary Layer, Boundary-Layer Meteorology, 132, 1–9, https://doi.org/10.1007/s10546-009-9385-3, https://doi.org/10.1007/s10546-009-9385-3, 2009.

Higgins, C. W., Froidevaux, M., Simeonov, V., Vercauteren, N., Barry, C., and Parlange, M. B.: The Effect of Scale on the Applicability of Taylor's Frozen Turbulence Hypothesis in the Atmospheric Boundary Layer, Boundary-Layer Meteorology, 143, 379–391, https://doi.org/10.1007/s10546-012-9701-1, 2012.

Higgins, C. W., Wing, M. G., Kelley, J., Sayde, C., Burnett, J., and Holmes, H. A.: A high resolution measurement of the morning ABL transition using distributed temperature sensing and an unmanned aircraft system, Environmental Fluid Mechanics, 18, 683–693, https://doi.org/10.1007/s10652-017-9569-1, https://doi.org/10.1007/s10652-017-9569-1, 2018.

Hinze, J.: Turbulence, McGraw-Hill Higher Education, New York, 1975.

Holtslag, A. A., Svensson, G., Baas, P., Basu, S., Beare, B., Beljaars, A. C., Bosveld, F. C., Cuxart, J., Lindvall, J., Steeneveld, G. J., Tjernström, M., and Van De Wiel, B. J.: Stable atmospheric boundary layers and diurnal cycles: Challenges for weather and climate models, Bulletin of the American Meteorological Society, 94, 1691–1706, https://doi.org/10.1175/BAMS-D-11-00187.1, 2013.

Izett, J. G., Schilperoort, B., Coenders-Gerrits, M., Baas, P., Bosveld, F. C., and van de Wiel, B. J. H.: Missed Fog?, Boundary-Layer Meteorology, https://doi.org/10.1007/s10546-019-00462-3, http://link.springer.com/10.1007/s10546-019-00462-3, 2019.

Jong, S. A. P. D., Slingerland, J. D., and Giesen, N. C. V. D.: Fiber optic distributed temperature sensing for the determination of air temperature, pp. 335–339, https://doi.org/10.5194/amt-8-335-2015, 2015.

Kaiser, R. and Knight, W.: Digital signal averaging, Journal of Magnetic Resonance (1969), 36, 215–220, https://doi.org/10.1016/0022-2364(79)90096-9, http://linkinghub.elsevier.com/retrieve/pii/0022236479900969, 1979.

Keller, C. A., Huwald, H., Vollmer, M. K., Wenger, A., Hill, M., Parlange, M. B., and Reimann, S.: Fiber optic distributed temperature sensing for the determination of the nocturnal atmospheric boundary layer height, Atmospheric Measurement Techniques, 4, 143–149, https://doi.org/10.5194/amt-4-143-2011, http://www.atmos-meas-tech.net/4/143/2011/, 2011.

Kelly, M., Wyngaard, J. C., and Sullivan, P. P.: Application of a Subfilter-Scale Flux Model over the Ocean Using OHATS Field Data, Journal of the Atmospheric Sciences, 66, 3217–3225, https://doi.org/10.1175/2009JAS2903.1, http://journals.ametsoc.org/doi/abs/10.1175/2009JAS2903.1, 2009.

Madhusudana, C.: Accuracy in thermal contact conductance experiments - the effect of heat losses to the surroundings, International Communications in Heat and Mass Transfer, 27, 877–891, https://doi.org/10.1016/S0735-1933(00)00168-8, http://linkinghub.elsevier.com/retrieve/pii/S0735193300001688, 2000.

Patton, E. G., Horst, T. W., Sullivan, P. P., Lenschow, D. H., Oncley, S. P., Brown, W. O. J., Burns, S. P., Guenther, A. B., Held, A., Karl, T., Mayor, S. D., Rizzo, L. V., Spuler, S. M., Sun, J., Turnipseed, A. A., Allwine, E. J., Edburg, S. L., Lamb, B. K., Avissar, R., Calhoun, R. J., Kleissl, J., Massman, W. J., Paw U, K. T., and Weil, J. C.: The Canopy Horizontal Array Turbulence Study, Bulletin of the American Meteorological Society, 92, 593–611, https://doi.org/10.1175/2010BAMS2614.1, http://journals.ametsoc.org/doi/abs/10.1175/2010BAMS2614.1, 2011.

Perry, A.: Hot-wire anemometry, Clarendon press, Oxford, UK, 1982.

Petrides, A. C., Huff, J., Arik, A., van de Giesen, N., Kennedy, A. M., Thomas, C. K., and Selker, J. S.: Shade estimation over streams using distributed temperature sensing, Water Resources Research, 47, https://doi.org/10.1029/2010WR009482, http://doi.wiley.com/10.1029/2010WR009482, 2011.

Sayde, C., Buelga, J. B., Rodriguez-Sinobas, L., El Khoury, L., English, M., van de Giesen, N., and Selker, J. S.: Mapping variability of soil water content and flux across 1-1000 m scales using the Actively Heated Fiber Optic method, Water Resources Research, 50, 7302–7317, https://doi.org/10.1002/2013WR014983, http://doi.wiley.com/10.1002/2013WR014983, 2014.

Sayde, C., Thomas, C. K., Wagner, J., and Selker, J.: High-resolution wind speed measurements using actively heated fiber optics, Geophysical Research Letters, 42, 10 064–10 073, https://doi.org/10.1002/2015GL066729, 2015.

Schilperoort, B., Coenders-Gerrits, M., Luxemburg, W., Jiménez Rodríguez, C., Cisneros Vaca, C., and Savenije, H.: Technical note: Using distributed temperature sensing for Bowen ratio evaporation measurements, Hydrology and Earth System Sciences, 22, 819–830, https://doi.org/10.5194/hess-22-819-2018, https://www.hydrol-earth-syst-sci.net/22/819/2018/, 2018.

Selker, J., van de Giesen, N. C., Westhoff, M., Luxemburg, W., and Parlange, M. B.: Fiber optics opens window on stream dynamics, Geophysical Research Letters, 33, 27–30, https://doi.org/10.1029/2006GL027979, 2006a.

Selker, J. S., Thévenaz, L., Huwald, H., Mallet, A., Luxemburg, W., Van De Giesen, N., Stejskal, M., Zeman, J., Westhoff, M., and Parlange, M. B.: Distributed fiber-optic temperature sensing for hydrologic systems, Water Resources Research, 42, 1–8, https://doi.org/10.1029/2006WR005326, 2006b.

Steele-Dunne, S. C., Rutten, M. M., Krzeminska, D. M., Hausner, M., Tyler, S. W., Selker, J., Bogaard, T. A., and van de Giesen, N. C.: Feasibility of soil moisture estimation using passive distributed temperature sensing, Water Resources Research, 46, https://doi.org/10.1029/2009WR008272, http://doi.wiley.com/10.1029/2009WR008272, 2010.

Taylor, G. I.: The Spectrum of Turbulence, Proceedings of the Royal Society A: Mathematical, Physical and Engineering Sciences, 164, 476–490, https://doi.org/10.1098/rspa.1938.0032, http://rspa.royalsocietypublishing.org/cgi/doi/10.1098/rspa.1938.0032, 1938.

Thomas, C. K., Kennedy, A. M., Selker, J. S., Moretti, A., Schroth, M. H., Smoot, A. R., Tufillaro, N. B., and Zeeman, M. J.: High-Resolution Fibre-Optic Temperature Sensing: A New Tool to Study the Two-Dimensional Structure of Atmospheric Surface-Layer Flow, Boundary-Layer Meteorology, 142, 177–192, https://doi.org/10.1007/s10546-011-9672-7, 2012.

Tsilingiris, P.: Thermophysical and transport properties of humid air at temperature range between 0 and 100°C, Energy Conversion and Management, 49, 1098–1110, https://doi.org/10.1016/j.enconman.2007.09.015, http://linkinghub.elsevier.com/retrieve/pii/S0196890407003329, 2008.

Tyler, S. W., Burak, S. A., McNamara, J. P., Lamontagne, A., Selker, J. S., and Dozier, J.: Spatially distributed temperatures at the base of two mountain snowpacks measured with fiber-optic sensors, Journal of Glaciology, 54, 673–679, https://doi.org/10.3189/002214308786570827, https://www.cambridge.org/core/product/identifier/S0022143000208770/type/journal{_}article, 2008.

Tyler, S. W., Selker, J. S., Hausner, M. B., Hatch, C. E., Torgersen, T., Thodal, C. E., and Schladow, S. G.: Environmental temperature sensing using Raman spectra DTS fiber-optic methods, Water Resources Research, 45, 1–11, https://doi.org/10.1029/2008WR007052, http://doi.wiley.com/10.1029/2008WR007052, 2009.

van de Giesen, N., Steele-Dunne, S. C., Jansen, J., Hoes, O., Hausner, M. B., Tyler, S., and Selker, J.: Double-ended calibration of fiber-optic raman spectra distributed temperature sensing data, Sensors (Switzerland), 12, 5471–5485, https://doi.org/10.3390/s120505471, 2012.

Webster, C. A. G.: A note on the sensitivity to yaw of a hot-wire anemometer, Journal of Fluid Mechanics, 13, 307, https://doi.org/10.1017/S0022112062000695, http://www.journals.cambridge.org/abstract{_}S0022112062000695, 1962.

Zeeman, M. J., Selker, J. S., and Thomas, C. K.: Near-Surface Motion in the Nocturnal, Stable Boundary Layer Observed with Fibre-Optic Distributed Temperature Sensing, Boundary-Layer Meteorology, 154, 189–205, https://doi.org/https://doi.org/10.1007/s10546-014-9972-9, 2015.

Žukauskas, A.: Heat Transfer from Tubes in Crossflow, pp. 93–160, https://doi.org/10.1016/S0065-2717(08)70038-8, http://linkinghub.elsevier.com/retrieve/pii/S0065271708700388, 1972.